UCRL-15465
S/C 8330003

CHARGED PARTICLE RESEARCH LABORATORY REPORT NO. 3-82

INVESTIGATION OF ELECTRON-BEAM CHARGING FOR INERTIAL-CONFINEMENT-FUSION TARGETS

UCRL--15465

DE82 017754

Scientific Report Prepared for
Lawrence Livermore National Laboratory

by

Kyekyoon Kim and Hani E. Elsayed-Ali

Charged Particle Research Laboratory
Department of Electrical Engineering
University of Illinois
Urbana, Illinois 61801

April 1982

CHARGED PARTICLE RESEARCH LABORATORY REPORT NO. 3-82

INVESTIGATION OF ELECTRON-BEAM CHARGING FOR INERTIAL-CONFINEMENT-FUSION TARGETS

Scientific Report Prepared for
Lawrence Livermore National Laboratory

by

Kyekyoon Kim and Hani E. Elsayed-Ali

Charged Particle Research Laboratory
Department of Electrical Engineering
University of Illinois
Urbana, Illinois 61801

April 1982

ABSTRACT

Techniques for charging inertial confinement fusion targets using electron beam are investigated. A brief review of the various possible charging techniques is presented, along with a discussion of the advantages and disadvantages of each. The reasons for selecting the electron beam charging and a physical picture of the charging mechanism are described. Experimental results are presented and compared with the theoretical predictions.

ACKNOWLEDGMENTS

We would like to express our gratitude to Dr. T. P. Bernat, Dr. C. D. Hendricks, and Dr. B. W. Weinstein of Lawrence Livermore National Laboratory, for their continuous support and interest in this work. This work was supported by the United States Department of Energy under the Lawrence Livermore National Laboratory Subcontract 8320003.

TABLE OF CONTENTS

LIST OF FIGURES

1. INTRODUCTION

1.1 Statement of Problem

Contactless handling of laser fusion targets, which allows for external observation, is needed for continuous production, selection, and injection of the targets for the inertial confinement fusion (ICF) power reactor systems. Levitation of particles by use of dielectrophoretic forces was previously investigated with the conclusion that for particles with higher permittivity than the surrounding media the required electric fields are too strong to make the method practical.[1]

Levitating charged particles using conventional electric quadrupole has been suggested for handling the laser fusion targets.[2] Because of the high resistivity of some of the ICF targets (for example, glass microballoon targets), accurate charging of targets poses a major problem in electrostatic levitation. Another problem arises due to the long charge relaxation time intrinsic to the target material which leads to slow distribution of charge over the target surface (e.g., for polystyrene and silicon glass $\tau = \frac{\varepsilon}{\sigma}$ is in the order of 10^5 s). Consequently, the charge imparted to one side of the target will take a long time before it distributes itself uniformly over the target surface. This, in turn, can reduce the accuracy of the pellet trajectory control.

The problem studied in this work is the charging of laser fusion targets using an electron beam. First, a brief review of the various possible charging techniques is presented, along with a discussion of the advantages and disadvantages of each. The reasons for selecting the electron beam charging method are given, which is followed by a description of the physical picture of the method. A theoretical model of the electron

beam charging is presented in Chapter 2 for the spherical targets. Chapter 3 is concerned with the apparatus used for the electron beam charging study. Experimental results obtained with this apparatus are presented in Chapter 4 and compared with the theoretical model of Chapter 2. Chapter 5 contains conclusions and recommendations for future work.

1.2 Possible Charging Methods

Techniques for charging high resistivity particles are numerous. Charging of high resistivity particles can be achieved using triboelectricity, induction charging, corona charging, and electron beam charging.[3, 4] Presented in what follows is a brief description of each of these charging techniques.

1.2.1 Triboelectricity

Triboelectricity is the charging of two materials as a result of the two coming in contact with each other. There are two effects involved in this charging process, the kinetic effect and the equilibrium effect. The kinetic effect results from asymmetric rubbing of two identical particles. As a stationary particle is rubbed asymmetrically by another identical particle, the rubbed section of the stationary particle is heated more than that of the moving particle resulting in transfer of electrons. Loeb studied this charging effect with the conclusion that its contribution is minor.[5] The equilibrium effect originates from static contact between two different materials. As two dissimilar materials are brought in contact, an electric field will be created due to the difference in the work functions of the two materials. If

the two materials brought in contact are dissimilar metals, there will be a transfer of electrons from one metal to the other in order to align the Fermi levels in both metals. In insulators the phenomenon of contact electrification is much more complicated and not well understood. This is due to the difficulties encountered in characterizing the energy levels in insulators and the charge trapping mechanism. Studies on contact charging have shown that it gives highly unreproducible results.[4] This disadvantage plus the possibility that it might incur damage on a laser fusion target during the charging process make this charging method unattractive.

1.2.2 Induction charging

Induction charging is the contact charging at high electric fields. Cho suggested the use of the simple charging configuration shown in Figure 1, where a highly resistive particle is placed on the bottom of a horizontal parallel-plate capacitor.[6] In this configuration a spherical particle will acquire the charge given by

$$Q = 1.65 \times 4 \pi \epsilon R^2 E_o \left[1 - \exp\left(\frac{-t}{\tau}\right)\right] \text{ coulombs}$$

where R is the radius of the particle being charged, E_o is the electric field intensity between the two plates in the absence of the particle, and τ is the charge transfer time constant ($\tau = \frac{\epsilon}{\sigma}$). As the particle gets charged, it will be accelerated upward and will go through the hole in the upper plate.

Although this method is simple to implement, it has the disadvantage

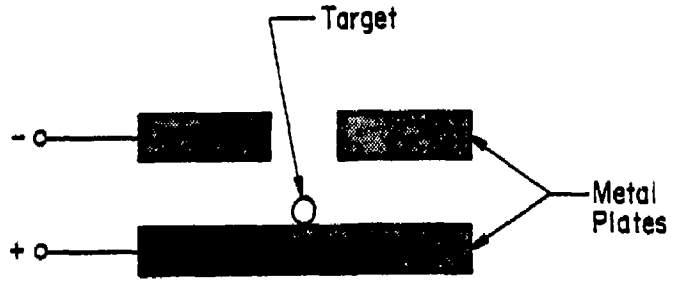

Figure 1. Induction charging.

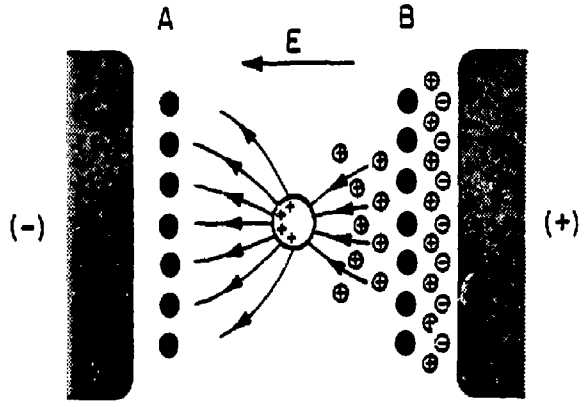

Figure 2. Corona charging.

of creating a nonuniform charge distribution over the surface of a highly resistive target.

1.2.3 Corona charging

In corona charging, targets are charged by placing them in an ionized gas medium consisting of particles predominantly of one polarity. Use of corona for the charging of laser fusion targets was suggested by Masuda, et al.[2, 7] As a result of applying an ac voltage between grids A and B shown in Figure 2, the ions generated at the two plates will move in one direction during the first half of a cycle and in the opposite direction during the other half. This will cause the target placed in a corona charging device, the "boxer charger," to be charged bidirectionally.[7]

In a uniform electric field, the maximum charge which can be imparted onto a spherical target due to ion bombardment is theoretically given by the Pauthenier's limit, $Q_{\infty p}$[8]

$$Q_{\infty p} = 4\pi\varepsilon_o \frac{3\varepsilon_s}{\varepsilon_s + 2} a^2 E$$

where a is the radius of the target, ε_s is the specific dielectric constant of the target material, and E is the electric field between the plates. However, for a particle with low ε_s the maximum charge will reach the Pauthenier's limit only if the target is bombarded by the ions uniformly in all directions. For the bidirectional charging as was suggested, the maximum charge for a target with ε_s=1 is 50% of the Pauthenier's limit.

This method of target charging is attractive because of its high

charging speed: the charge on the target reaches its maximum limit in the order of tens of milliseconds. However, several disadvantages are encountered in this method. The need of a high-pressure gas for the generation of corona discharge demands that a differential pumping stage must be installed before the charged targets could be injected into the reactor chamber which is maintained at high vacuum. Charging at high pressures will also speed up the decay process of the charge already on the target, resulting in loss of charge. In addition to these problems, from the standpoint of pellet trajectory control, a non-trivial problem of the corona charging method is that it lacks in the control over the depth, density, and lateral distribution of the resulting charge of the target.[9]

1.2.4 Electron beam charging

Electron beam charging of a target can be achieved by bombarding it with energetic electrons that have ranges less than the dimensions of the target. Because electron beam charging offers many advantages compared to the other methods, it was chosen as the method to be investigated for the present work.

Electron beams can be created in high vacuum using thermionic emission, for example. They can also be made to propagate through regions having different pressures by using a thin metal foil or even a thin silicon window which is fabricated to be transparent to electrons, but designed to block the gas flow between the chambers at different pressures.[10] This eliminates the need for a differential pumping stage in the pellet transport system. In addition, electron beam charging offers a fine control over charge depth, charge density, and lateral

charge distribution in the target.[9] Because electron beam charging of a target is a result of injecting electrons into it, the charge imparted to the target, provided that it is protected from ionizing radiation, is highly stable for a long time (in order of years) if the target is kept in high vacuum and at room temperature.[11] Another advantage of the electron beam charging is that electrons require much less energy than ions of equal range. Thus less damage is caused to the target by the electron beam charging than the ion beam charging. Because of the high uniformity of the laser fusion targets required for successful target implosion, this advantage of the electron beam charging compared to corona charging can prove to be particularly significant.

1.3 Physical Picture of Electron Beam Charging

As illustrated by Figures 3.A and 3.B, when the primary electrons strike the surface of a target, they release some secondaries due to the process of secondary electron emission, leaving initially a positively charged surface layer. The number of secondary electrons released for every primary electron is called the secondary emission yield or secondary emission coefficient, which depends on the electron energy and the surface properties of the target. For most polymers, the secondary emission yield reaches a maximum of 2-5 at a primary electron energy of 150-300 eV and decreases as V^{-1} at higher energies.[3] As the primary electrons penetrate into the target, they generate electron-hole pairs and lose energy through collisions. As a result, the primary electrons come to rest in a fairly well-defined range. The electron-hole pairs generated are of relatively small energy and, consequently, most of them become quickly trapped. The process of electron-hole generation increases the

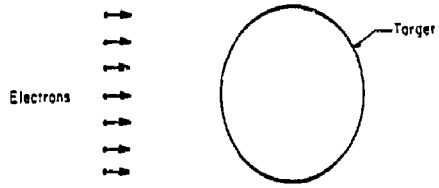

A. Target before electron beam bombardment

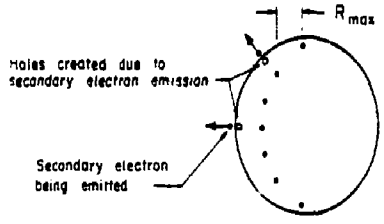

B. Electrons are injected into the target to their maximum range (R_{max})

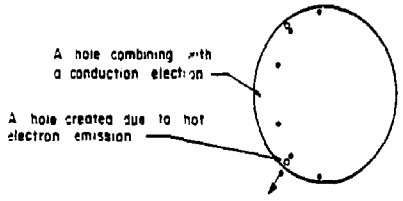

C. Electrons move towards the target surface

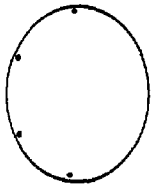

D. Electrons are finally trapped near the target surface

Figure 3. Physical picture of electron beam charging.

conductivity of the irradiated region, which is called the "radiation induced conductivity (RIC)."[12]

As time goes on, the injected electrons accumulate in a well defined range inside the target and develop an internal electric field. The internal field developed between the injected charge layer and the surface of the target will accelerate part of the free carriers generated during irradiation and heat them as their energy is randomized due to collisions. A simplified model of electron heating in solids due to an applied field predicts that the electron temperature will be much greater than the lattice temperature.[13] As a result, hot electrons near the surface of the target will be emitted, leaving a layer of positive charge in addition to the positive charge that was created due to the secondary electron emission as the primary electrons bombarded the surface of the target. This process is illustrated in Figure 3.C.

As electron beam bombardment of the target continues, two processes occur which intensify the field between the injected charge layer and the surface of the target. First, more hot electrons are emitted from the surface which increases the charge in the positive surface charge layer and which, in turn, increases the field between the surface of the target and the injected charge layer. Such an increase in the internal field creates more emission of hot electrons from the surface of the target. Consequently, the internal field increases. Because of this positive feedback process, when the internal field reaches a high value, a sharp decrease in the field external to the target

(that is, the superposition of the fields created by the positive surface charge layer and the negative electron layer) would result. This external field could vanish when the field due to the positive surface charge layer cancels the field due to the negative injected electron layer.[14]

Second, because of the radiation induced conductivity (RIC) created in the irradiated region and because of the internal field between the positive surface charge layer and the negative injected electron layer, the injected electron layer moves towards the surface. This process is called the "range reduction" and is also illustrated in Figure 3.C. As a result of this range reduction process, the internal field is increased as was shown by Gross.[15] This increase in the internal field, in turn, speeds up the range reduction process resulting in a positive feedback.

In order to retain the negative charge trapped in the target after termination of the bombardment by the electron beam, it is necessary to inject more negative charge into the target than the positive surface charge created at a specific time of irradiation. When the charging process is terminated, the range reduction process will still continue because of the delayed radiation induced conductivity (DRIC). When the injected electron charge layer reaches the surface of the target, part of it will neutralize the positive surface charge layer and the remaining negative charges will be trapped near the surface of the target as illustrated in Figure 3.D.

2. THEORY OF ELECTRON BEAM CHARGING

A theory explaining the time development of the field external to an electron-irradiated dielectric was presented by Watson and Dow.[14] The semiqualitative theory presented here is an adaptation of their theory applied to spherical targets and includes, in addition, the effect of secondary electron emission from the target surface and the effect on the bombarding electrons of the charge already on the target.

The time development of the magnitude and configuration of the trapped charge in the target depend on the factors listed below:

1. The energy of the bombarding electrons.
2. The current density of the electron beam.
3. The effect of the secondary electron emission current from the surface of the target.
4. Hot electron emission current from the surface of the target.
5. Conduction current of the injected electrons moving toward the target surface.
6. Recombination of positive and negative charges near the surface of the target.

The effect of each of these factors (1 through 6) will be discussed in order of their appearance. This discussion will then be followed by the necessary mathematical formulation.

1. In order that the bombarding electrons be trapped inside the target, the electron beam range must be less than the thickness of the target. Otherwise, electrons will hit the target from one side, penetrate through it and escape from the opposite side. The range of electrons in a specific material depends on the electron energy. An

investigation of the range of low-energy electrons in solids was presented by Holliday and Sternglan.[16] Adjusting their results to a density of 1 g/m^3 (which is a good approximation for the density of glass used in the fabrication of laser fusion targets and the density of polystyrene used in this experiment), Cross and Blake[17] obtained a plot of the range of electrons as a function of electron energy as shown in Figure 4. In this figure it is shown that for a bombarding electron energy of 10 keV the range of electrons in the target is less than 4 μm, which is less than the thickness of most types of laser fusion targets.

2. The obvious effect of the change in the current density of the electron beam is the proportional change in the rate of electron injection into the target. However, an increase in the electron current density will also increase the effects of Factors 3 through 6 discussed in the foregoing. Therefore, it should not be assumed that for a constant electron energy and charging time an increase in the current density of the electron beam will always increase the charge trapped in the target. The overall effect of the current density of the bombarding electrons will be discussed later in this chapter.

3. As the target is bombarded by the electron beam, some electrons get knocked off the surface of the target by the process of secondary electron emission. The secondary electron emission coefficient depends on the energy of the bombarding electrons. For very low energies

$$\delta = F_1 U$$

where U is the energy of the bombarding electrons, and

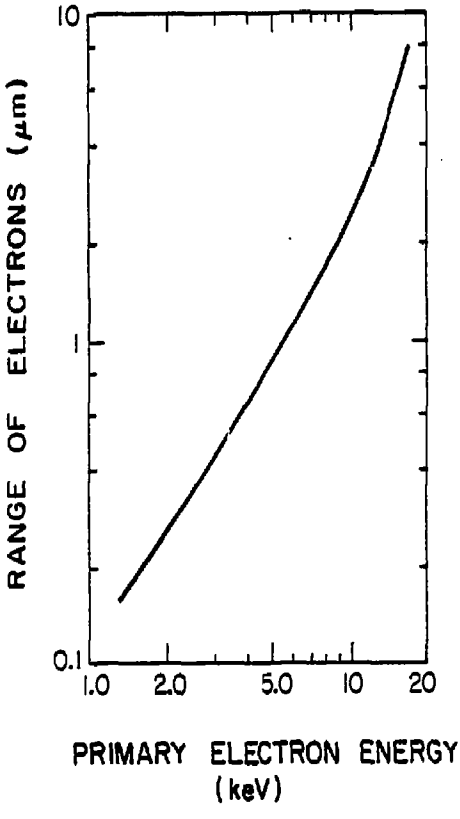

Figure 4. Range of electrons vs. primary electron energy for material density of 1 g/cm^3.

F_1 is a constant which depends upon the excitation energy required to produce a secondary electron and upon the amount of absorption of secondaries.

The energy of the bombarding electrons, U, is determined not only by the energy gain of the electrons in the absence of the target placed in the beam, but also by the effect of the electric field produced by the charge on the target. In order to account for this effect, the electric field just outside the target is represented by E_s. Then, it is possible to represent the effect of the charged target on the energy of the bombarding electrons by

$$-F_2 |E_s|$$

where F_2 is a constant which depends on the distance between the target and the source of the electrons. Now, the energy of the bombarding electrons upon reaching the surface of the target is given by

$$U = U_o - F_2|E_s|$$

where U_o is the energy of the electrons when the target is not charged, i.e., when $E_s = 0$. For very low energies of the bombarding electrons, the secondary electron emission coefficient is

$$\delta = F_1(U_o - F_2|E_s|) \tag{2.1a}$$

For high energy of the bombarding electrons, the secondary electron emission coefficient is given by

$$\delta = \frac{F_1F_3}{U} = \frac{F_4}{(U_o - F_2|E_s|)} \tag{2.1b}$$

where F_3 is a constant which depends on the density of the material and

$$F_4 = F_1 F_3$$

Therefore, as seen above, as the target is being bombarded with primary electrons, there will be secondary electrons leaving the surface of the target. The current density due to the emission of these secondary electrons, J_{sec}, is given by the relation

$$J_{sec} = J\delta \tag{2.1c}$$

where J is the magnitude of the current density of the bombarding electron beam.

4. Another significant variable affecting the charging process is the hot electron emission from the surface of the target. A simplified model of electron heating in an electric field predicts that electron temperature, T_e, exceeds the lattice temperature, T, such that [13]

$$T_e - T = \alpha E^2$$

Just inside the surface of the target, the value of T_e can be approximately

$$T_e \simeq \alpha E_s^2$$

where α is a constant.

Substituting this for T_e in the Richardson-Dushman equation for hot electron emission[18]

$$J_e = A_1 |E_s| \exp(-B_1/E_s^2) \tag{2.2}$$

where J_e is the current density due to hot electron emission,

A_1 is an experimentally determined constant dependent on the material of the target, and B_1 is a constant which depends on the work function of the material of the target.

5 and 6. The other two factors affecting the electron beam charging of the target are the conduction current from the injected electrons to the surface of the target and the recombination of positive and negative charges near the surface of the target. The magnitude of the conduction current, J_c, is given by

$$J_c = -\frac{|E_s|}{\rho}$$

where ρ is the resistivity of the dielectric. The conductivity of the dielectric is a function of electron temperature and is given by[19]

$$\frac{1}{\rho} = \frac{1}{\rho_o} \exp\left(-\frac{\phi}{KT_e}\right) = \left(\frac{1}{\rho_o}\right) \exp\left(-\frac{B_2}{E_s^2}\right)$$

where ρ_o is a constant of the dielectric, and B_2 is a constant depending on the depth of the electron trap, ϕ, below the conduction band. The rate of recombination of positive and negative charges at the surface of the target, which is characterized by the recombination current, J_r, depends on the conduction current, J_c, and the surface charge density, σ_a,

$$J_r = \alpha_r \sigma_a J_c \qquad (2.3a)$$

where α_r is the recombination coefficient. For a uniform spherical surface charge distribution, the surface charge density, σ_a, is given by

$$\sigma_a = \varepsilon E_a \tag{2.3b}$$

where E_a is the electric field just outside the target due to the surface charge only, and ε is the permittivity of the target material. The external field just outside the target, E_s, is the superposition of E_a and the electric field from the injected charges just outside the target, E_s.

$$|E_s| = |E_a| - |E_i|$$

Now

$$J_r = \varepsilon\alpha_r(|E_s| + |E_i|)\,|E_s|\,(\frac{1}{\rho_o})\,\exp\,(-\frac{B_2}{E_s^2}) \tag{2.3c}$$

The rate of change of E_s is given by

$$\dot{E}_s = \dot{E}_a + \dot{E}_i = \frac{\dot{\sigma}_a}{\varepsilon} + \dot{E}_i$$

The rate of change of the surface charge density is given by

$$\dot{\sigma}_a = J_e + J_{sec} - J_r$$

From Eqs. (2.1), (2.2) and (2.3), σ_a is given by

$$\dot{\sigma}_a = A_1|E_s|\,\exp\,(-\frac{B_1}{E_s^2}) + JF_1(U_o - F_2|E_s|)$$
$$- \frac{\varepsilon\alpha_r}{\rho_o}\,(|E_s| + |E_i|)\,|E_s|\,\exp\,(-\frac{B_2}{E_s^2}) \tag{2.4a}$$

when U has a very low value, and

$$\dot{\sigma}_a = A_1|E_s| \exp\left(-\frac{B_1}{E_s^2}\right) + \frac{JF_4}{(U_o - F_2|E_s|)} - \frac{\varepsilon\alpha_r}{\rho_o}\left(|E_s| + |E_i|\right)|E_s| \exp\left(-\frac{B_2}{E_s^2}\right) \tag{2.4b}$$

when U has a high value.

The field component due to the injected electrons in the target, E_i, depends on the range of the electrons. In turn, the range of electrons in the target depends on the external field and the conductivity of the target. An investigation of the field due to the injected charge taking into account the range reduction effect was undertaken by Gross.[15] In order not to further complicate the expression for $\dot{E}_s$, the field component due to the injected electrons will be taken to vary linearly with time,[14] namely,

$$E_i = -(\eta t - G|E_s|t) = -(\eta + GE_s)\, t \tag{2.5}$$

where η is a constant depending on the electron injection rate, and G is a constant depending on the location of the target in the electron gun.

The electron bombardment energy, U, depends on the energy gain of the electrons if the target is not placed in the electron beam and on the external electric field due to the charge on the target. In the present experiment, the energy gain of electrons due to anode potential is considerably higher than 300 eV. Therefore, at low values of E_s, the energy of the bombarding electrons, U, will not be greatly affected by the charge on the target and, consequently, will have a high value. From (2.4b) and (2.5)

$$\dot{E}_s = \frac{A_1}{\varepsilon}|E_s| \exp\left(-\frac{B_1}{E_s^2}\right) + \frac{JF_4}{\varepsilon(U_o - F_2|E_s|)} - \frac{\alpha_r}{\rho_o}\left(|E_s| - (\eta - G|E_s|)t\right)|E_s| \exp\left(-\frac{B_2}{E_s^2}\right) - \frac{d}{dt}(\eta + GE_s)t \tag{2.6}$$

At low values of E_s, the terms in $\dot{E}_s$ that represent the hot electron emission current and the recombination current are negligible. Also, the effect of the field due to the charge on the target can be neglected in the secondary electron emission term and in the electron injection term. Therefore,

$$\dot{E}_s = \frac{JF_4}{\varepsilon U_o} - \eta$$

with the boundary condition $E_s = 0$ at $t = 0$. Therefore,

$$E_s = \left[\frac{JF_4}{\varepsilon U_o} - \eta\right] t$$

But, from the physical picture presented in the last chapter, it was explained that the delayed radiation induced conductivity, DRIC, and the internal field of the target will cause the injected electron layer to continue to move towards the surface of the target after the termination of the electron beam bombardment. Some of these electrons will combine with the holes near the surface of the target and the rest of the electrons will be trapped near the surface. Therefore, the net charge on the target, Q, is given by

$$Q = 4\pi R^2 \varepsilon_o \left[\frac{JF_4}{\varepsilon U_o} - \eta\right] t \qquad (2.7)$$

where R is the radius of the target. Equation (2.7) establishes the form of the growth of the injected electron charge with time for small values of Q.

At high values of E_s the bombarding electron energy, U, will be small because of the retarding effect of the field external to the target due to the injected charge. Therefore, from Eqs. (2.4a) and (2.5)

$$\dot{E}_s = \frac{A_1}{\varepsilon} |E_s| \exp\left(-\frac{B_1}{E_s^2}\right) + \frac{JF_1}{\varepsilon}(U_o - F_2|E_s|) -$$

$$\frac{\alpha_r}{\rho_o}(|E_s| - (\eta - G|E_s|)t)\,|E_s| \exp\left(-\frac{B_2}{E_s^2}\right) - \frac{d}{dt}(\eta + GE_s)t \qquad (2.8)$$

When E_s has a high value, the exponents in $\dot{E}_s$ will approach units. Therefore,

$$\dot{E}_s = \frac{1}{1+Gt}\left[\left(\frac{\alpha_r}{\rho_o}Gt + \frac{\alpha_r}{\rho_o}\right)E_s^2 + \left(\frac{A_1}{\varepsilon} - \frac{JF_1F_2}{\varepsilon} + \frac{\alpha_r}{\rho_o}\eta t + G\right)|E_s| - \eta + \frac{JF_1}{\varepsilon}U_o\right]$$

This nonlinear differential equation determines the behavior of E_s as a function of time for large values of E_s. The charge in target, Q, is given by

$$Q = 4\pi R^2 \varepsilon_o E_s$$

Therefore, for large values of Q

$$\dot{Q} = \frac{4\pi R^2 \varepsilon_o}{1+Gt}\left[\left(\frac{\alpha_r}{\rho_o}Gt + \frac{\alpha_r}{\rho_o}\right)E_s^2 + \left(\frac{A_1}{\varepsilon} - \frac{JF_1F_2}{\varepsilon} + \frac{\alpha_r}{\rho_o}\eta t + G\right)|E_s| - \eta + \frac{JF_1}{\varepsilon}U_o\right]$$

No attempts will be made here to solve the above differential equation. Instead, the experimental results given in Chapter 4 determine the general behavior of the charge injected into target Q as a function of electron beam bombardment time, t. In addition, using the form of Q as a function of time t derived theoretically in this chapter plus the obtained differential equation of Q as a function of t for large values of Q, a discussion will be made later to explain the obtained experimental results.

3. EXPERIMENTAL APPARATUS AND TECHNIQUES

The experiment apparatus and techniques used in the electron beam charging study are presented in this chapter. Two electron guns with different current ranges were constructed. In Section 3.1, a description of the construction, operation, and limitations of the thermionic emission electron gun is given. A description of the hollow cathode electron gun is presented in Section 3.2 along with its basic principle of operation and an experimental investigation of the energy distribution of the extracted electrons. The high voltage pulsers used in the operation of the electron guns are described in Section 3.3. In order to measure the charge on a target, a Faraday cage was used. A description of this Faraday cage and the amplifier circuit is presented in Section 3.4 along with the calibration techniques for the Faraday cage.

3.1 The Thermionic Emission Electron Gun

An electron gun capable of generating currents of a few microamperes to several milliamperes was constructed and is shown in Figure 5. The basic physical process in the operation of this electron gun is thermionic emission. As the temperature of the tungsten filament is raised by electrical heating, some of the electrons in the conduction band gain sufficient energies to overcome the surface potential energy barrier. The energy of these emitted electrons resulting from the heating of the filament will have a Maxwellian distribution. However, this component of the electron energy is negligible as at a filament temperature of 2000 K more than 99.99% of the emitted electrons have energies less than 2 eV.[18] The current density of the emitted

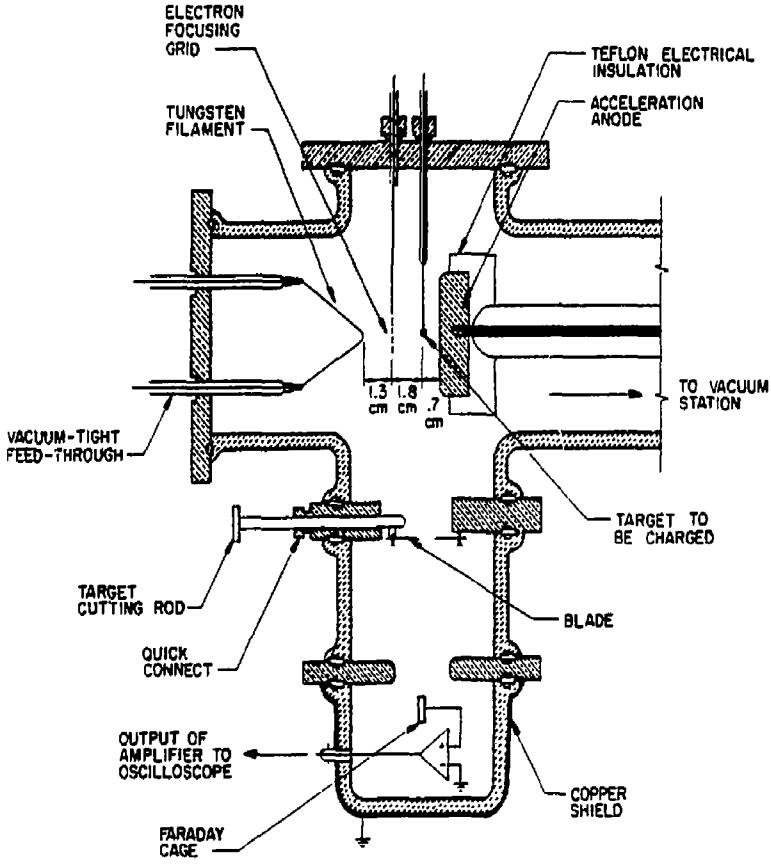

Figure 5. The thermionic emission electron gun.

electrons is a function of the temperature and the work function of the filament material, and is given by the Richardson-Dushman equation.

$$J_e = A_e T^2 \exp(-e\phi/KT)$$

where J_e is the current density of the emitted electrons (A/m^2)

A_e is an experimentally determined constant (72 for tungsten)

K is the Boltzmann's constant (1.38×10^{-23} W.s/K),

ϕ is the work function (eV),

T is the absolute temperature, and

e is the electronic charge (-1.60×10^{-19} coulomb).

The emitted electrons are accelerated by the potential at the anode through the grid which focuses the electron beam and therefore acts as an electron lens. The focusing grid was made out of 0.108 mm-diameter stainless steel wire mesh with 0.108 mm spacing between the wires. The grid was made circular with a diameter of 1.2 cm and was spot-welded to a stainless steel ring for electrical connection. The ring was placed between two insulating teflon rings.

The anode was made in the shape of a flat circular disk with a diameter of 3.2 cm and was electropolished in order to minimize possibilities for gas breakdown. The electrical connections to the vacuum chamber were made through a kovar metal-to-glass seal.

The electron gun assembly was mounted on a vacuum station consisting of a forepump connected to a diffusion pump and a liquid nitrogen cryotrap. In order to greatly decrease the number of ions bombarding the cathode, it was necessary to evacuate the system to very low pressures. A vacuum in the order of 1×10^{-5} torr was used during the charging process. The vacuum was measured using the ionization and thermocouple gauges.

The cathode filament was fabricated out of tungsten wires of variable thicknesses to obtain a range of electron beam current densities. The filament was heated using a Variac autotransformer connected to a filament transformer as shown in Figure 6.

The focusing grid was grounded through a 1.5 MΩ resistor. The circuits used for high voltage pulsing of the anode will be described later in this chapter.

3.2 The Hollow Cathode Electron Gun

3.2.1 Basic principle of operation

In order to obtain an electron beam of high current density, a hollow cathode electron gun capable of delivering electron beam pulses of current densities of the order of tens of A/cm^2 was constructed as shown in Figure 7. The electron beam device basically consists of three major regions: (1) the plasma generation region where the electrons are created in the hollow cathode; (2) the extraction and control regions where the electrons are extracted from the plasma through the grid anode G_1 and where their energy is controlled by the control grid G_2; and (3) the acceleration (or drift) region where the electrons propagate due to the energy gain resulting from the cathode-anode potential difference only, or as a result of the cathode-anode potential difference and the energy supplied to the electrons by the accelerating anode.[20]

The plasma generation region is the volume surrounded by the hollow cathode and the grid anode G_1. A cross section through the hallow cathode perpendicular to its axis is shown in Figure 8, along with the potential and electric field distributions inside the hollow cathode. A key feature in the construction of the hollow cathode is that the surface area of the

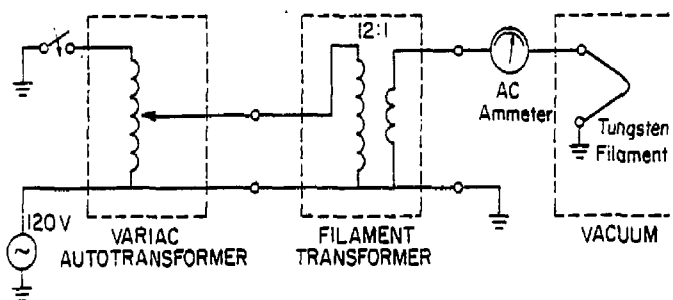

Figure 6. Filament heater circuit.

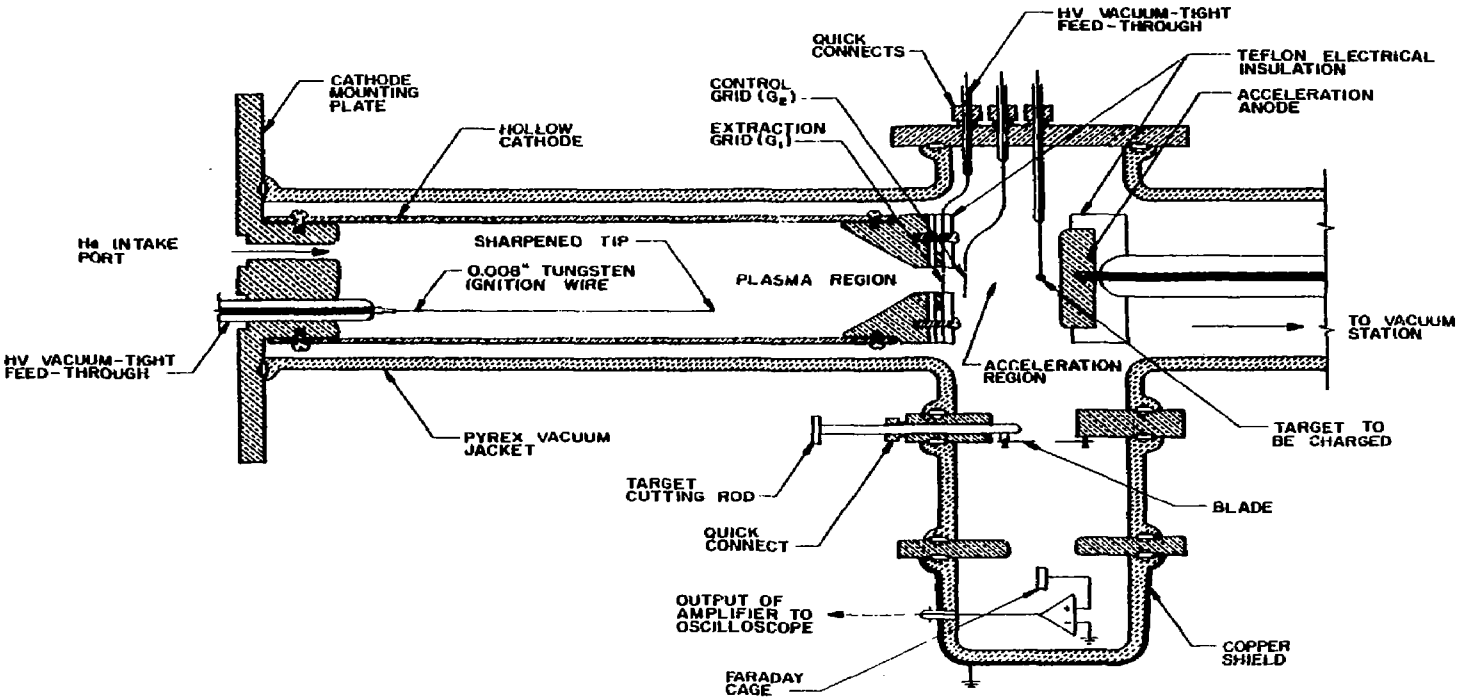

Figure 7. The hollow cathode electron gun.

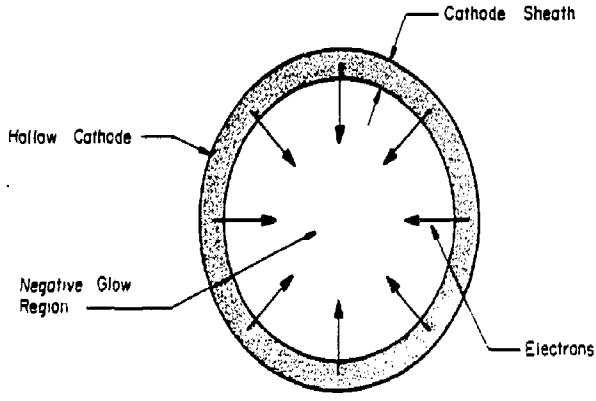

(a) Cross Sectional View of the Hollow Cathode

(b) Potential Distribution Across the Diameter of the Hollow Cathode

(c) Electric Field Distribution Inside the Hollow Cathode

Figure 8. A cross section throughout the hollow cathode demonstrating the hollow cathode effect.

cathode surrounding the plasma is much larger than that of the anode. With a large cathode-to-anode area ratio, most ions leaving the negative glow region are accelerated through the cathode sheath and utilized with large efficiency for the production of secondary electrons from the surface of the cathode. In addition, electrons leaving the surface of the cathode will be rapidly accelerated by the large electric field of the cathode sheath region and will contribute to ionization in both the cathode sheath and negative glow regions. These additional electrons will also be accelerated by the electric field in the cathode sheath region. Some electrons will hit the opposite side of the cathode and create secondary electron emission or will cause electrons to escape from the surface of the cathode by the Auger process. In the Auger process the primary electrons have sufficient energies to remove electrons from the K-shells of the atoms which subsequently results in X-ray radiation due to the dropping of the electrons in the outer shells (L, M, N, etc.) to the K-shell. This radiation is absorbed, instead of being emitted, by some of the outer shell electrons which, in turn, gain sufficient energy to escape. As seen from the above discussion, the larger the cathode-to-anode area, the larger the efficiency for the trapping of electrons and ions. However, it should be pointed out that the distance between the two opposite sides of the cathode, i.e., the diameter of the hollow-cylindrical cathode, must be large enough to allow for the cathode sheath region to form. It is also worthwhile to mention that some studies have suggested that the main mechanism responsible for the hollow cathode effect is the photo ionization which is enhanced by the geometric effect of the hollow cathode.[21]

In operating the hollow cathode electron gun, He gas was used as

the fill gas because He^+ ions have relatively low sputtering yield which increases the life span of the device.

Electrons created inside the hollow cathode are extracted through the grid anode G_1. The control grid G_2 serves the purpose of varying the energy of the extracted electron beam.

The acceleration region, where the target to be charged is placed, is the region between G_2 and the accelerating anode. The width of this region is a critical parameter, and must be small to avoid Paschen breakdown. For example, at He pressure of 60 millitorr and an applied voltage of 10 kV between the control grid G_2 and the accelerating anode, the width of the accelerating region must be less than 4 cm in order to avoid a breakdown.

As noted before, the sustainment of the hollow cathode discharge is dependent upon the existence of a sufficient number of ions and electrons to be reflected back and forth in the hollow cathode. At an operating pressure as low as 60 millitorr, such a plasma will not be formed simply by applying a cathode-anode voltage. In the absense of this plasma, electrons initially present in the hollow cathode (by photoionization, for example) will be captured by the cathode without experiencing ionizing collisions. To solve this problem, an igniter wire fabricated out of tungsten was introduced to permit initiation of the hollow cathode discharge without having to apply excessively high voltages between the cathode and the anode.[22] The igniter tip was sharpened to 9-μm diameter. Because of the high electric field near the tip of the igniter wire, a local breakdown gets initiated. Such a breakdown increases the number of electrons and then increases the probability for ionization collisions.

3.2.2 Construction of the device

The hollow cathode was made out of a stainless steel tube which was electropolished. The length of the cathode was 29 cm and the inside diameter was 3.7 cm. The extraction area is equal to the area of the anode grid exposed to the discharge plasma and was 1 cm^2. The grid anode was made out of a stainless steel wire mesh with wire diameter of 0.184 mm. The spacing between each wire was 0.216 mm. The electrical connections were inserted into the vacuum chamber through a kovar metal-to-glass seal as in the case of the thermionic emission gun (Section 3.1). The accelerating anode used in this electron gun was the same anode that was used in the thermionic electron gun. The electron gun assembly was mounted on the same vacuum station used before.

3.2.3 Determination of the relative energy of the extracted electrons

A retarding potential technique was employed to determine energy spread of the extracted electron beam. A negative voltage applied to the control grid G_2 was used to retard the electrons extracted from the hollow cathode. Because of the simplicity of the DC operation in varying the retarding potential, the measurements were taken under the DC mode of operation. Clearly, the obtained electron beam energy distribution would also apply to pulsed operation.

The voltage applied to each electrode and the value of the resistance through which it is applied are indicated in Figure 9. In order to create a pressure gradient such that the pressure in the drift region is less than the pressure inside the hollow cathode, an electric valve was used to puff the helium gas into the cathode.

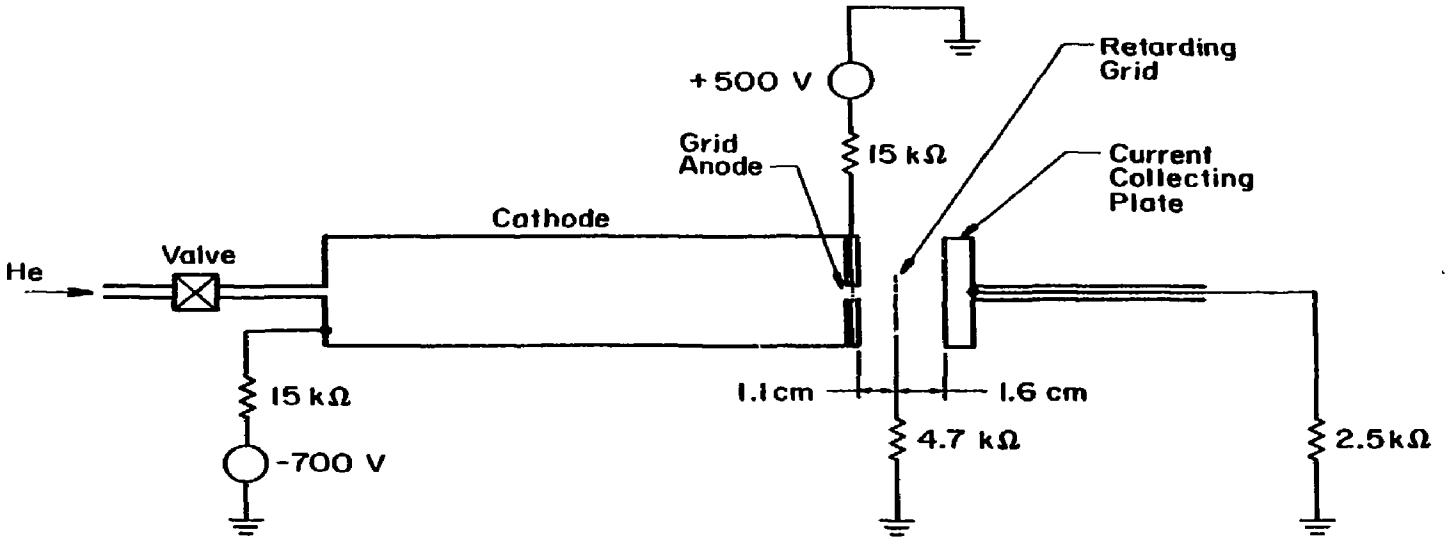

Figure 9. Schematic of circuit used in determining the energy distribution of the extracted electrons from the hollow cathode.

The system was evacuated to a pressure in the order of 1×10^{-5} torr. Then the voltages were applied to the electrodes as shown in Figure 9. Because of the very low operating pressure, no discharge occurred and, consequently, no current flowed in any of the electrodes. By applying a voltage pulse to the control circuit of the electric valve, a burst of helium gas was introduced inside the cathode such that the pressure in the drift region was less than 30 millitorr. Upon introduction of helium gas into the system, electron current flowed in the current collecting plate creating a voltage drop across the 2.5 kΩ resistor. As helium gas was pumped out, the flow of electrons stopped and, therefore, an electron beam pulse was obtained. The duration of the electron beam pulse depended on the amount of gas introduced into the hollow cathode and on the pumping capacity of the vacuum system. The puffing of helium gas into the hollow cathode and the measurement of the voltage drop across the 2.5 kΩ resistor were repeated for different control grid voltages. The percentage ratios of the electron beam currents, obtained at various control grid voltages, to the maximum electron beam current (i.e., the current obtained at no applied retarding potential) are given in Table I and plotted in Figure 10.

From Table I and Figure 10 it is apparent that as the control grid voltage goes more negative, more electrons are repelled and the current collected by the current collecting plate decreases. The amount of current collected by the plate reached a minimum at about 0.96 mA. Therefore, it is conjectured that this current was due to existence of ions in the drift region. Since the current was measured with no retarding voltage at 7.4 mA, it is concluded that electrons comprised 87% of this current, and the rest consisted of ions.

Table I

Determination Of Relative Electron Beam Energy

Retarding potential (V_{G_2}) (Volts)	Electron beam current (I_c) (mA)	$[I_c/I_{cMAX}](\%)$
0	7.4	100
-50	7	94.6
-100	6.5	86.5
-150	5.6	75.7
-200	5	67.6
-250	4.52	61.1
-300	4	54.1
-350	3.28	44.3
-400	2.52	34.1
-450	2.08	28.1
-500	1.8	24.3
-550	1.4	18.9
-600	1.06	14.3
-700	.96	13.0

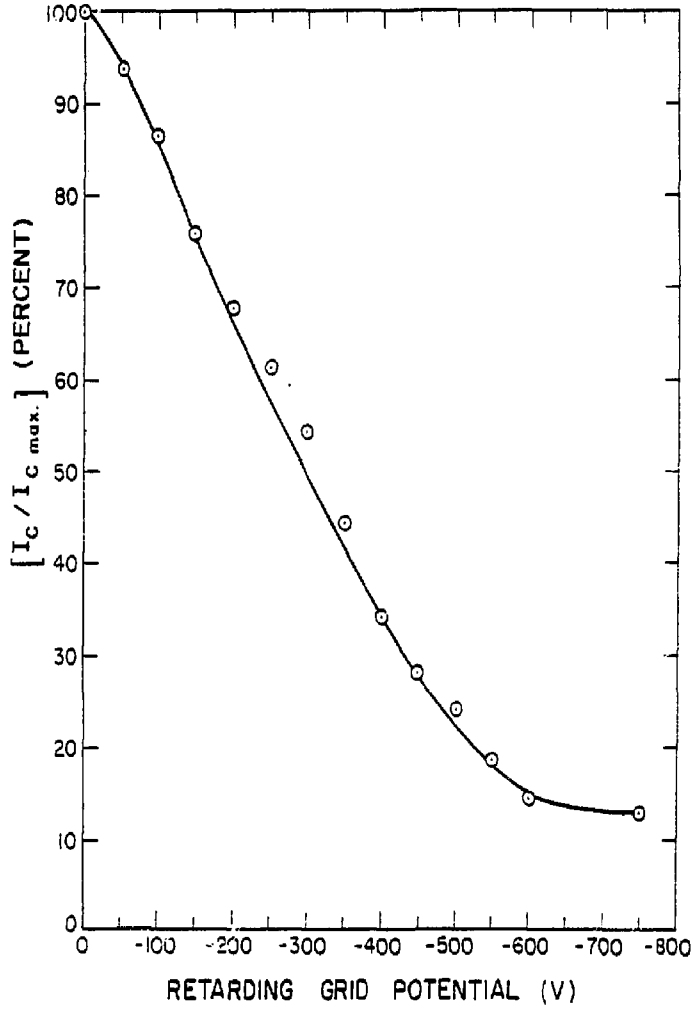

Figure 10. Percentage ratio of the electron beam currents at various control grid voltages.

3.3 The High Voltage Pulsers

Two high voltage pulsers were constructed. The first pulser was solely for pulsing high voltages to the anode of the thermionic emission electron gun. A diagram of this circuit is shown in Figure 11. This high voltage pulser consists of a 3310A Hewlett-Packard function generator being operated in pulse generator mode. By pulsing the base of the 2N6308 transistor, current passes through the coil of the relay which closes the circuit that activates the high voltage relay switch connecting the output of the high voltage power supply to the anode. The pulse width is variable and depends on the width of the pulse generated by the function generator. Because of the finite mechanical response time of the relays, very short pulses cannot be obtained using this circuit. The maximum amount of current drawn out of this pulser equals the maximum current output of the high voltage power supply used. In the present work, the maximum current that could be obtained was 50 mA.

The second high voltage pulser constructed was capable of delivering very short pulses ($\simeq$ .2 ms width with output "open circuit"). When this circuit was used to pulse the hollow cathode electron gun, electron beam current pulses had a maximum amplitude of the order of tens of amps. The current pulse width was in the order of tens of microseconds and depended on the amount of loading provided to the electrodes. A diagram of this high voltage pulser is given in Figure 12. The 2-μF capacitor is charged to the power supply voltage through the 3.9 mΩ resistor. When the thyratron tube was fired, this capacitor would discharge through the thyratron tube. The thyratron used was a Kuthe Laboratories 5C22 which was triggered by a pulse generated by a

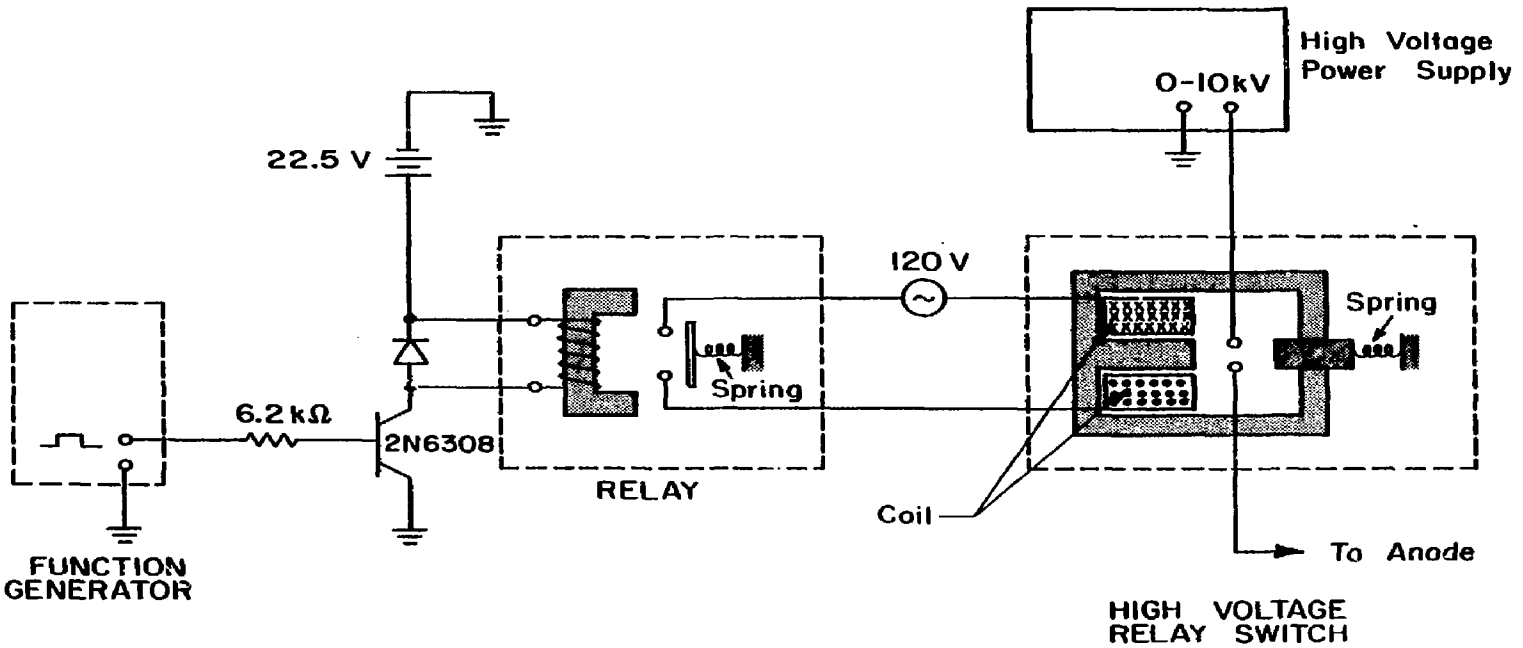

Figure 11. Relay switch high voltage pulser.

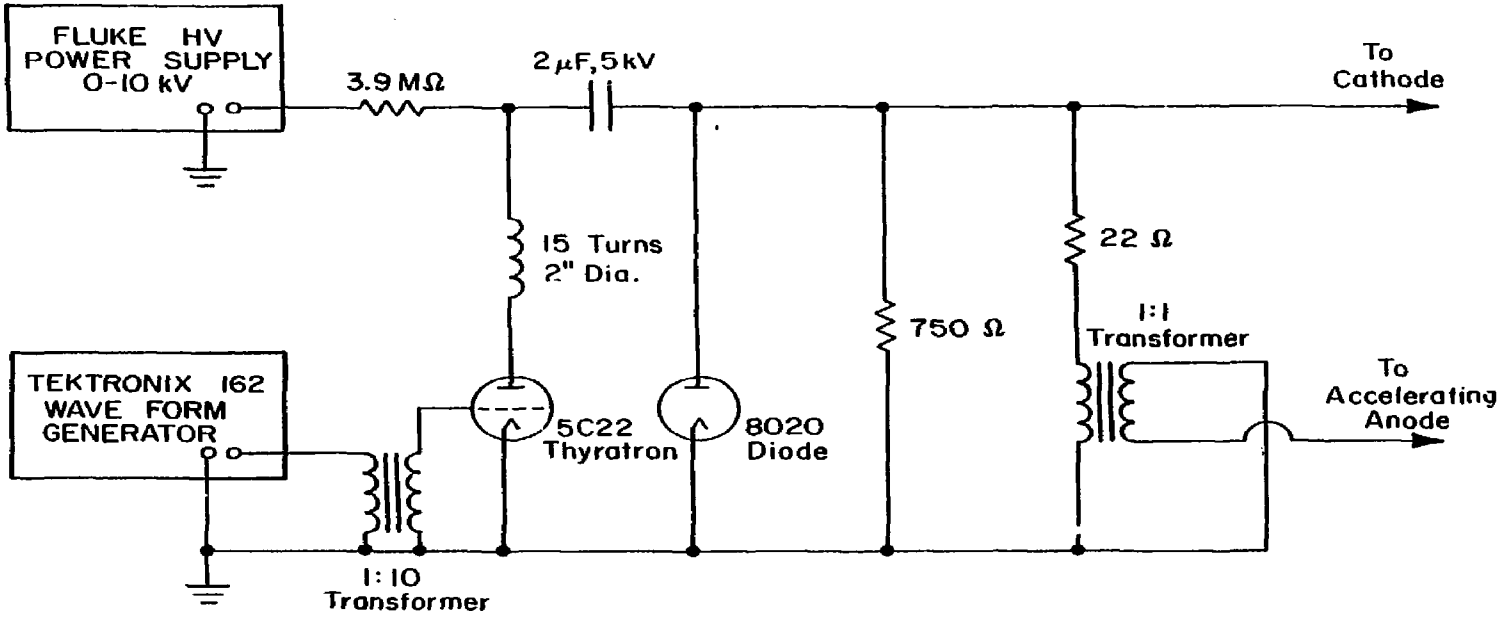

Figure 12. Thyratron operated high voltage pulser.

Tektronix 162 wave form generator after being amplified by a transformer. A 1:1 iron core transformer was used to invert the output pulse in order to obtain a positive pulse. The diode 8020 tube has the function of protecting the 5C22 thyratron from any possible negative pulses going to its anode.

3.4 Charge Measurement Technique

3.4.1 Description of the charge measuring device--A Faraday cage

To measure the charge on the targets a Faraday cage was used. Details of the Faraday cage and amplifier circuit are shown in Figure 13. The basic principle of operation of the Faraday cage is the electrostatic induction. As a charged target passes through the Faraday cage, it induces an image charge on the copper tube comprising the Faraday cage. Assuming that all the field lines originating from the target terminate at the tube, the image charge induced on the outer surface of the tube equals the charge on the target and has the same polarity; consequently, the input capacitance C_{in} is charged with the same charge and polarity as the target. It is this voltage across C_{in} that is measured by the oscilloscope after being multiplied by the gain of the amplifier. A Raytheon brand CK5886 subminiature electrometer pentode operated as a triode was used in a cathode follower configuration to provide very low leakage current (maximum control grid current = 2.5×10^{-13} A) without a substantial reduction in the gain of the amplifier.

The input capacitance C_{in} must be low, since for a given amount of charge, smaller capacitance gives higher voltage (V=Q/c). However, the input resistance R_{in} must be large enough to allow for the time of

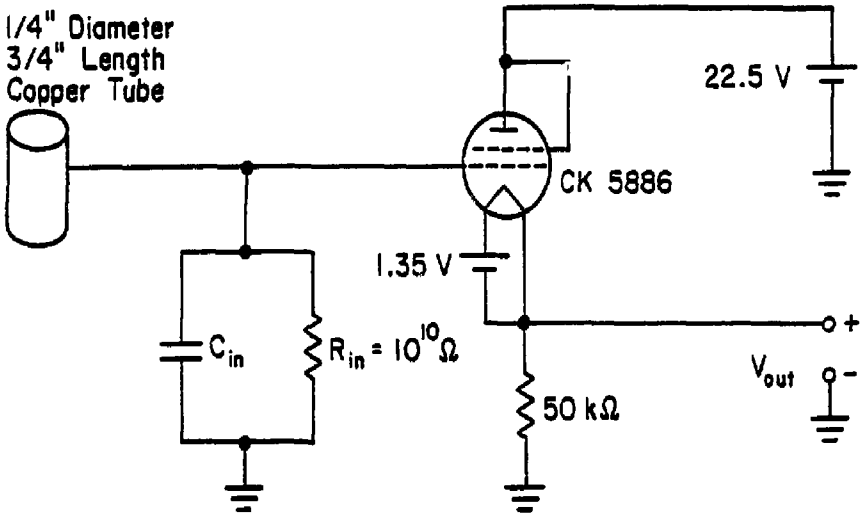

Figure 13. Faraday cage and amplifier circuit.

flight of the target through the tube, t_1, to be much shorter than the time required for C_{in} to discharge, t_2,

$$t_2 >> t_1 = R_{in}C_{in}$$

3.4.2 Calibration of Faraday cage

The input capacitance C_{in} must be measured in order to determine the charge induced on the Faraday cage. To measure C_{in}, a known capacitance C_k is connected between the output of a signal generator and the Faraday cage tube as shown in Figure 14. At high frequency the impedance of C_{in} is negligible compared with R_{in}. Therefore, C_{in} can be determined by the relation

$$C_{in} = C_k \frac{GV_{in} - V_{out}}{V_{out}}$$

The gain of the amplifier, G, was measured for different values of input voltage V_{in} as shown in Figure 15 and the mid-band frequency of the amplifier, G_{mid}, was found to be .6. From the relation given above C_{in} was determined to be 22.26 pF.

3.4.3 Target charging and determination of charge on target

The target to be charged was glued onto a 10-um thick glass fiber and then bombarded with the electron beam. After termination of this charging process, the target was lowered just below the cutting knife, and the glass fiber to which the target was connected was cut so that the target would fall through the Faraday cage. The output of the Faraday cage amplified circuit was measured using a storage oscilloscope.

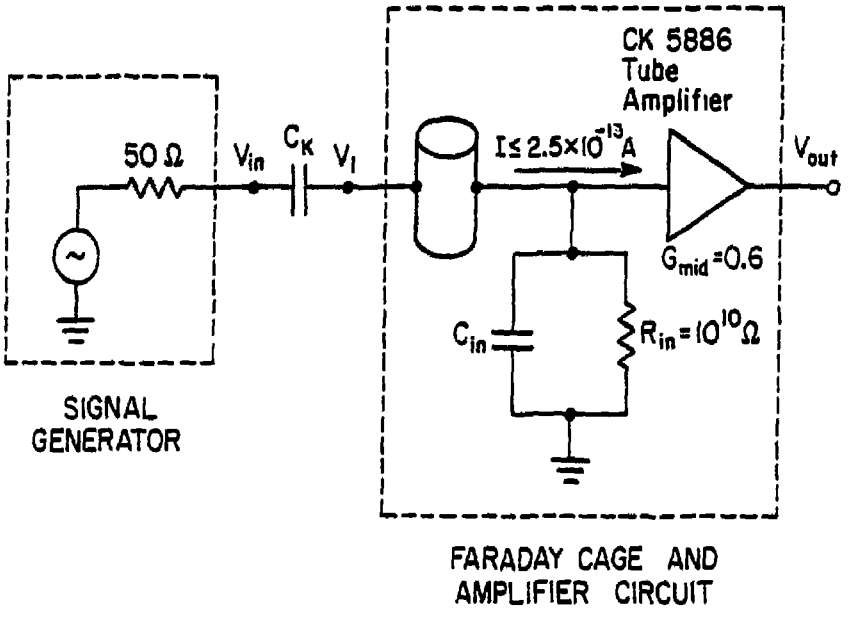

Figure 14. Calibration of Faraday cage.

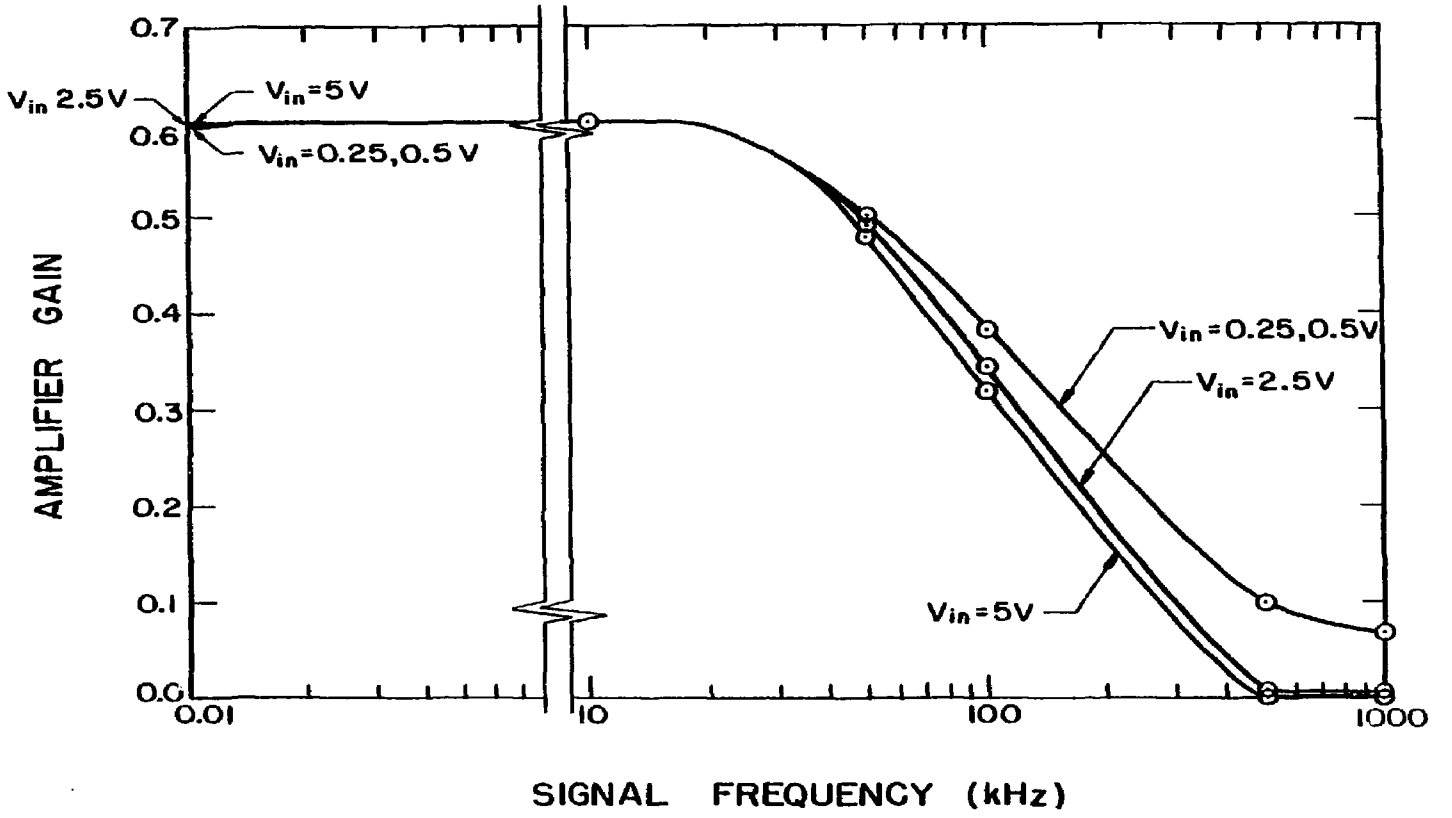

Figure 15. Gain of cathode follower amplifier for different values of input voltages.

4. EXPERIMENTAL RESULTS AND DISCUSSION

Electron beam charging of laser fusion targets was investigated with the following objectives: first, to determine the amount of charge on target as a function of charging time and beam currents; second, to study the maximum possible charge on target for different electron energies; and third, to investigate the effects of the ambient pressure on the stability of charge on the target. The targets used in this work were polystyrene spheres, and had a density of 1.050 kg/m^3. The diameters of the targets were measured by a microscope and varied from 406 to 540 μm.

4.1 Charge on Target as a Function of Charging Times for Different Electron Beam Currents

The electron beam used for the charging of targets was generated by the thermionic emission electron gun described in Chapter 3. Electrons created at the cathode filament were accelerated by 3.9 kV pulses applied to the anode. The time duration of the anode voltage pulse was 6.1 s which is equal to that of the electron beam pulse. The pressure of the charging chamber was kept as low as $1x10^{-5}$ torr. The electron beam current was varied by controlling the amount of current supplied to the cathode filament using the Variac autotransformer. The average current density of the electron beam can be obtained by dividing the amount of current measured at the anode by the area of the focusing grid which was 1.13 cm^2.

Each target was bombarded with a known number of electron beam pulses. After termination of the electron beam bombardment, the charge on the target was measured by dropping the target through the Faraday Cage.

The mass of each target was calculated using the measured value of its diameter and its known density, allowing for the calculation of the charge-to-mass ratio. This procedure was repeated for a various number of electron beam pulses with currents of 6, 20 and 28 mA. The results are plotted in Figures 16, 17 and 18, and tabulated in Appendix I.

As shown in Figure 16, the amount of charge on the target increases as the target is bombarded with an increasing number of electron beam pulses. For small values of electron beam bombardment time, t, it is shown that the injected electron charge, Q, increases linearly with t. This linear behavior was established theoretically in Chapter 2. For small Q, the charge-to-mass ratio was, therefore, given by

$$\frac{Q}{m} = \frac{-4\pi\varepsilon_o R^2}{m} \left[\eta - \frac{JF_4}{\varepsilon U_o}\right] t \qquad (4.1)$$

This expression was obtained as superposition of two effects: the injection of electrons into the target which gave the term $-\frac{4\pi\varepsilon_o R^2}{m}[\eta]$ and the creation of a positive surface charge layer due to secondary electron emission. This process resulted in the term

$$\frac{4\pi R^2}{m} \frac{JF_4}{\varepsilon U_{ro}} t$$

Because of the high electron energy, U_o, used in the current investigation, the secondary electron emission part in Eq. (4.1) will be, for small Q, much smaller than the part due to the electron injection. In addition, the parameter η depends on the rate of electron injection into the target and, therefore, is directly proportional to the electron beam current density, J. As a result, as the electron beam current density increases, the slope of $\frac{Q}{m}$ plotted as a function of t for small

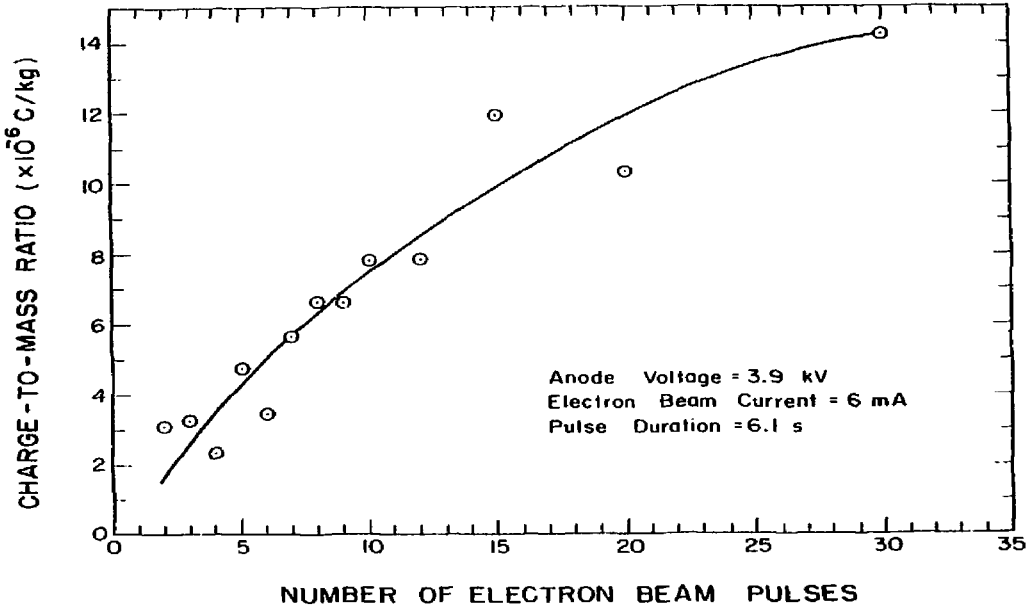

Figure 16. Charge on target vs. number of electron beam pulses for electron beam current of 6 mA.

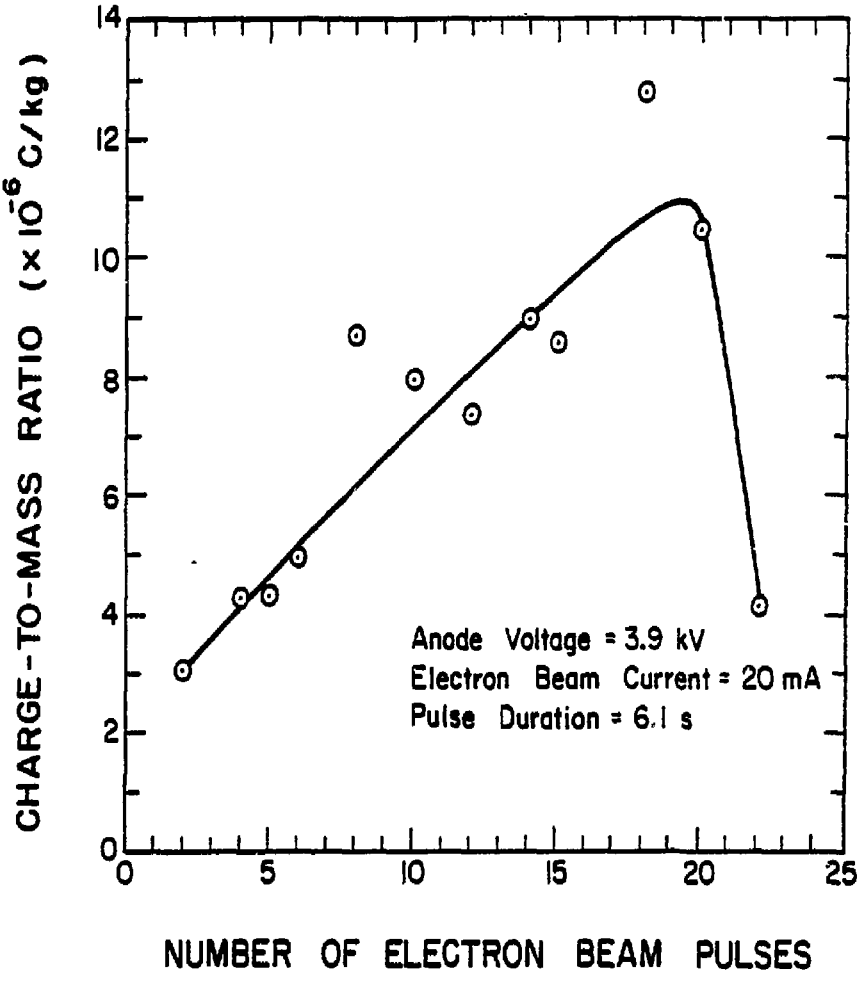

Figure 17. Charge on target vs. number of electron beam pulses for electron beam current of 20 mA.

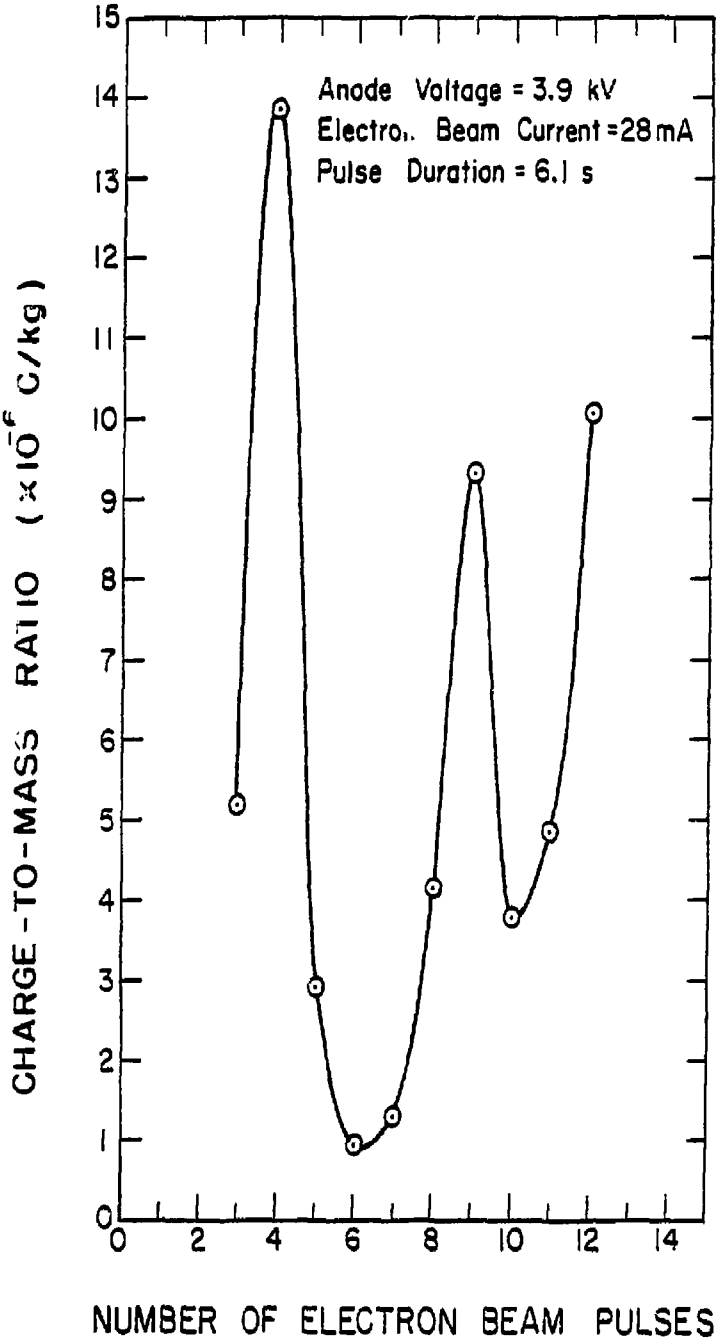

Figure 18. Charge on target vs. number of electron beam pulses for electron beam current of 28 mA.

Q would increase. This result was verified experimentally as shown in Figures 16, 17 and 18. At a very high electron beam current (28 mA), the slope is almost vertical as shown by Figure 18.

For low electron beam currents, as the number of electron beam pulses bombarding the target increases, the amount of charge imparted to the target reaches a saturation point as shown in Figure 16 for an electron beam current of 6 mA. Referring back to Chapter 2, the charge imparted to the target, Q, for large values of Q is given by

$$\dot{Q} = \frac{4\pi R^2 \varepsilon_o}{1 + Gt} \left[-\left(\frac{\alpha_r}{\rho_o} Gt + \frac{\alpha_r}{\rho_o}\right) E_s^2 + \left(\frac{A_1}{\varepsilon} - \frac{JF_1F_2}{\varepsilon} + \frac{\alpha_r}{\rho_o} \eta t + G\right) |E_s| - \eta + \frac{JF_1}{\varepsilon} U_o \right] \tag{4.2}$$

The saturation point of Q is, therefore, reached when the negative and positive terms in Eq. (4.2) are equal, namely, when the electron injection rate is reduced by the retardation effect of the charge on the target and when the secondary electron emission and hot electron emission currents balance the recombination current.

When the targets were bombarded with an electron beam with high current density, an interesting phenomenon was observed to occur. As the number of electron beam pulses was increased, a certain point was reached where a sudden decrease in the amount of charge on the target occurs. From Figures 17 and 18, it is seen that this reduction of charge occurs sooner as the current density of the electron beam increases. In particular, it is seen from Figure 18 that, when the number of electron pulses was further increased, the cycle of charge build-up and sudden decrease repeated itself and appeared to have a well-behaved periodic nature. This behavior is consistent with the physical picture presented in Chapter 1, as at a certain point, there will occur a positive feedback mechanism by which an increase in the internal field

of the target (that is, the field between the positive surface charge layer and the injected electron layer) causes an increase in the hot electron emission from the surface of the target, which increases the internal field. The higher the electron beam current density, the sooner this process occurs. It is responsible for the charge release that was observed.

Similar behavior was observed by Watson and Dow[14] where flat samples made out of different dielectric materials were irradiated with a 2 MeV electron beam. At very low rates of electron beam injection, the field measured external to the sample grew linearly at small charging time and finally reached a saturation point. At a higher rate of electron beam injection, periodic collapses of the external field were observed accompanied by an emission of high-frequency current transients which was explained by hot electron emission from the surface of the sample.

As was mentioned earlier, at small charging time, an increase in the current density of the bombarding electrons will increase the rate of electron injection into the target. Consequently, an increase in the current density of the bombarding electron beam will speed up the charging process. An experiment was performed in order to investigate the charging process as a result of bombarding the target with an electron beam having very high current density (in the order of tens of A/cm^2) and very short pulse duration (in the order of tens of microseconds). The short pulse duration was desirable in order to try to prevent the charge release effect observed before when the current density of the electron beam was increased. An electron beam with such high current density was possible to obtain using the hollow cathode electron gun. Details concerning this electron gun and the thyratron

operated high voltage pulser that was used to pulse the various electrodes of the electron gun were given in Chapter 3.

During the operation of the electron gun, helium gas was introduced inside the cathode such that the pressure in the accelerating region was less than 30 millitorr. The current density of the extracted electron beam depended on the applied voltages and the resistance loading of the various electrodes. By varying the electron beam current density and electron energy, several attempts were made to charge the targets. Targets were bombarded with as much as 50 electron beam pulses; however, no charge was measured on the targets. This result is probably due to loss of charge by the process of hot electron emission from the surface of the target as was observed in Figures 17 and 18.

4.2 Maximum Charge on Target for Different Electron Energy

A set of experiments was performed to determine the effect of the electron energy on the maximum charge injected into the target. The thermionic emission electron gun was used with the electron beam current set at 6 mA. The pressure in the system once again kept as low as 1×10^{-5} torr. The electron energy was varied by applying different voltages to the anode. The electron beam pulses were of 6.1 s duration. Each target was bombarded with 30 pulses, which, as was observed in Sec. 4.1, were sufficient to charge the targets to a value near the saturation limit. The charge on the target was measured using the same method as before, from which the charge-to-mass ratio was calculated. The results thus obtained are plotted in Figure 19 and are also tabulated in Appendix I.

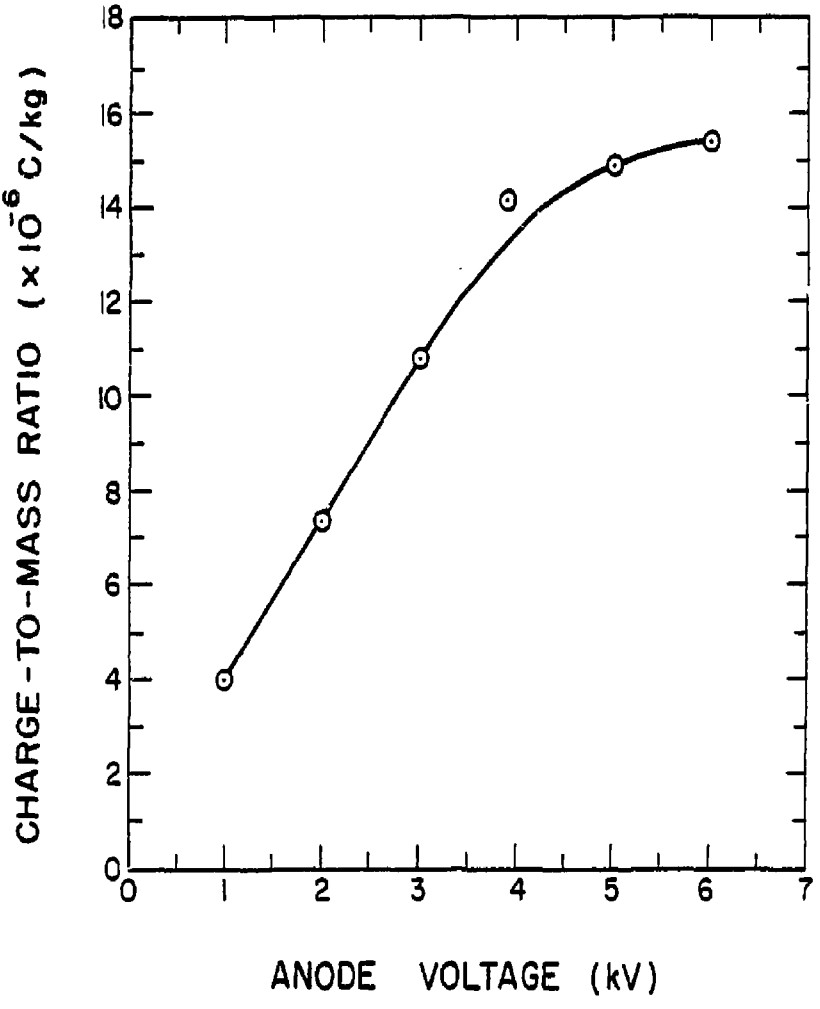

Figure 19. Maximum charge on target vs. electron energy.

In Figure 19 the charge-to-mass ratio is shown first to increase linearly with the applied anode voltage and then reach a saturation point. The linear increase of the charge-to-mass ratio is explained by referring to Figure 4 where it is shown that as the primary electron energy increases the range of the electrons inside the target also increases. Such an increase in the range of electrons will decrease the internal field between the negative electron layer and the positive surface charge layer, which, in turn, decreases the amount of hot electron emission from the surface of the target. Another effect caused by the increase in the electron energy is the decrease in the amount of electron backscattering at the target surface. The effect of electron backscattering was not included in the theory presented; however, it does play a role in the charging process. An increase in the primary electron energy will result in an increase in the secondary electron emission at high values of Q. This effect was considered in Chapter 2 and is given by the last term of $\dot{Q}$, where

$$\dot{Q} = \frac{4\pi R^2 \varepsilon_o}{1 + Gt}\left[\left(\frac{\alpha_r}{\rho_o} Gt + \frac{\alpha_r}{\rho_o}\right) E_s^2 + \left(\frac{A_1}{\varepsilon} - \frac{JF_1F_2}{\varepsilon} + \frac{\alpha_r}{\rho_o}\eta t+G\right)|E_s| - \eta + \frac{JF_1}{\varepsilon} U_o\right]$$

An increase in the primary electron energy, U_o, will also raise the rate of electron loss at the target surface. This process might be the one responsible for the saturation effect observed in Figure 19.

4.3 Charge on Target as a Function of Ambient Pressure

An experiment was performed to investigate the charge release process from the target as a function of the ambient pressure. The

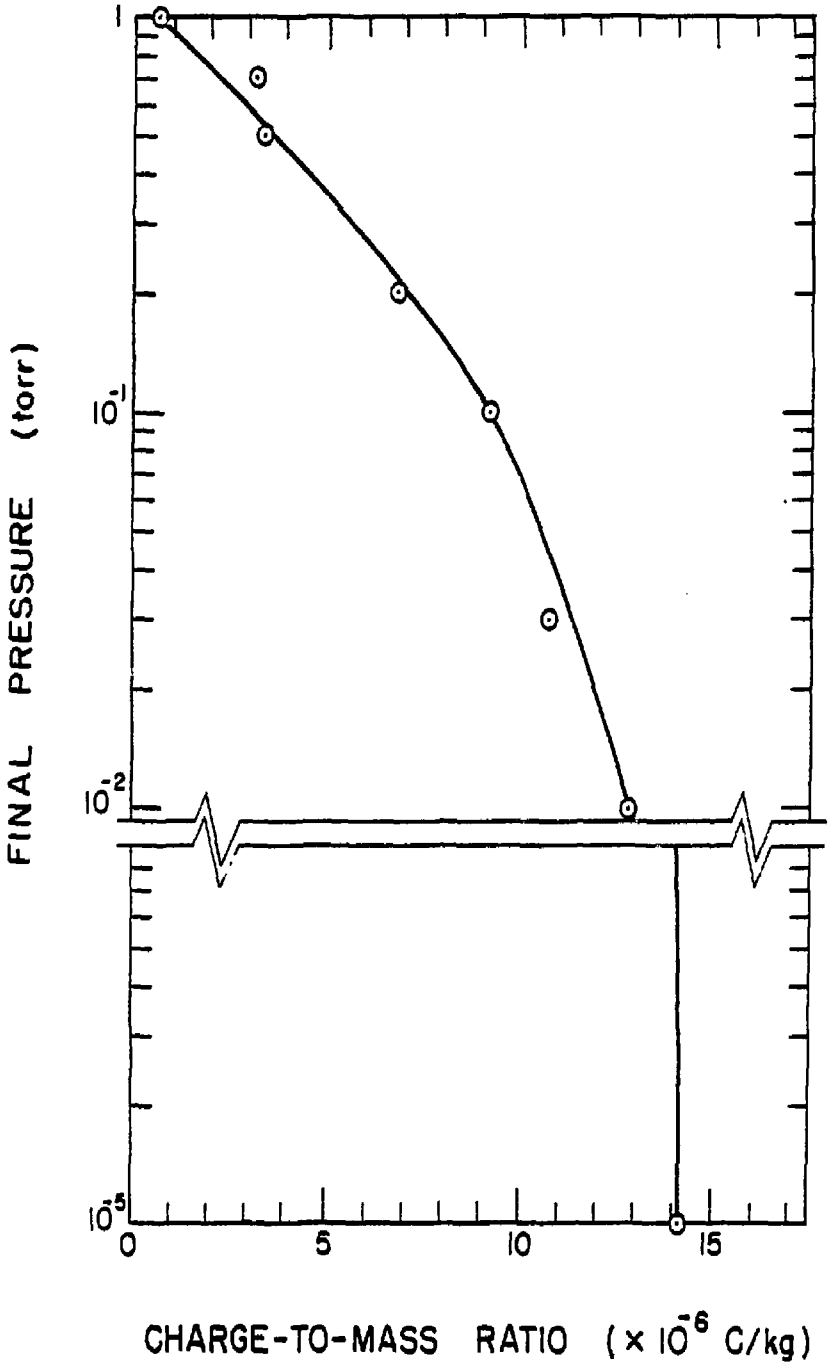

Figure 20. Charge on target vs. ambient pressure.

thermionic emission electron gun was used to produce an electron beam current of 6 mA. A 3.9 kV pulse of 6.1 s duration was applied to the anode. Each target was charged to a value near its saturation limit by bombarding it with 30 electron beam pulses. During the charging process, the pressure in the system was kept as low as $1x10^{-5}$ torr. After termination of the charging process, air was first introduced into the system to a specific pressure. The charge on target was then measured by dropping it through the Faraday cage. The results thus obtained are plotted in Figure 20 and tabulated in Appendix I.

As shown in Figure 20, as the pressure of the air surrounding the charged target is increased from 10^{-5} torr to 10^{-2} torr, the release of charge from the target is seen to be insignificant. However, as the pressure surrounding the target is further increased, the charge decay process is accelerated. For example, at a pressure of 1 torr, less than 5% of the original charge on the target remains trapped. In order to understand this phenomenon, it is worthwhile to have a quick review of the charge decay process in dielectrics.

The decay of injected charges in dielectrics is due to either internal or external process. The internal process is due to the drift of injected charges by their own field and the diffusion of excess charges by their random motion which has the effect of decreasing the concentration gradients of charges. The external process is due to the attraction of charges of a different polarity which compensate for the injected charges. The external process is also due to the attraction of polar molecules such as water, which, although not carrying net charges, enhances the decay of charges in the dielectric by the internal decay process.

The lifetime of the charge on the target was found to be long if the target was kept at a high vacuum. No noticeable decrease in the charge-to-mass ratio was measured when targets charged to a value close to their saturation charge were kept at a pressure of 1×10^{-5} torr for a period of 50 minutes. This is an indication that the internal charge decay processes are very small if the targets are kept in high vacuum. The instantaneous charge release process of the target that was observed when the pressure of the surrounding media was increased is mainly due to the recombination of the negative injected charges of the target with the positive ions in the air. However, because of the existence of water molecules in the air, it is likely that an enhancement of the drift process will result and have some effect on the charge decay process.

5. CONCLUSIONS AND RECOMMENDATIONS

In this investigation, the feasibility of an electron beam for laser fusion target charging has been assessed by bombarding spherical polystyrene targets with an electron beam, having a current density of a few milliamperes per square centimeter and electron energy of a few kilovolts; a maximum charge-to-mass ratio of approximately 15×10^{-6} C/kg was achieved. The behavior of the charge on the target as a function of electron beam bombardment time was investigated for different electron beam current densities. At low electron beam current densities, the charge on the target reached a saturation value if the target was bombarded with the beam long enough. At higher current densities, however, a sudden reduction in the amount of charge was to occur after it had first reached a maximum value. As the charging time was further increased, the process of charge trapping and sudden release was repeated in a periodic fashion. This phenomenon of charge release occurred earlier as the current density of the electron beam was increased.

A semiqualitative theoretical model of electron beam charging was presented in Chapter 2. The observed sudden charge release was attributed to the accelerated hot electron emission and secondary electron emission from the surface of the target.

The charge on the target was highly stable as long as the target was kept in a low-pressure environment. As the ambient pressure was increased, a reduction in the amount of charge began to occur. The amount of charge released was found to accelerate as the pressure was increased. At pressures higher than 1 torr, the amount of residual charge on the target was seen to be almost negligible.

Possible techniques for charging high resistive particles were described in Chapter 1. The selection of the electron beam as the means for charging laser fusion targets was mainly due to the fact that it is the most likely candidate for achieving uniform charging and for incurring the least damage on the target surface. For further investigation, it is suggested that an in-depth experimental analysis be carried out to compare the damage done on the target surface by the electron beam charging and other possible charging methods (for example, corona charging).

In order to increase the amount of charge which ends up on the target, use can be made of the phenomenon of radiation hardening. Radiation hardening is a phenomenon in which the amount of charge captured by a dielectric is increased by subjecting it to a massive dose of radiation. Such a phenomenon was observed when a dielectric was subjected to heat irradiation, which is considered to generate additional traps.[23] Other radiation hardening effects were observed when Teflon was irradiated with a dose of the order of 100 Mrad using a scanning electron beam and observed to considerably increase the stored charge.[12] This observation was attributed to the decrease in the delayed radiation induced conductivity (DRIC) which acts as a loss mechanism after termination of the charging process.

In order to improve the stability of the charge on the target, several methods are suggested as being worthwhile to investigate. For example, it has been demonstrated that application of heat during electron beam charging increases the stability of the injected charges.[24] Heating the dielectric after charging results in some loss of charge; however,

the remaining charge is considered to be more stable. By repeatedly charging and heating a dielectric, the total amount of injected charges increases and its stability improves.[25] Also, heating prior to charging has been shown to improve stability of the charge.[26] Such effects of heating on the charge stability are attributed to the generation of deep traps, or, in the case of heating during the electron irradiation, to the retrapping of charges in deeper energy levels.

APPENDIX I

TABULATED EXPERIMENTAL DATA

1. Charge on target vs. time for different electron beam currents.

Anode voltage = 3.9 kV

Electron beam pulse duration = 6.1 s

A. Electron beam current = 6 mA

Mass of target ($\times 10^{-7}$ kg)	Number of e-beam pulses	Total e-beam bombardment time (s)	Charge on target ($\times 10^{-12}$ C)	Charge-to-mass ratio ($\times 10^{-6}$ C/kg)
5.33	2	12.2	1.67	3.13
5.87	3	18.3	1.89	3.22
5.48	4	24.4	1.30	2.37
5.51	5	30.5	2.60	4.72
5.41	6	36.6	1.86	3.44
3.94	7	42.7	2.23	5.66
6.14	8	48.8	4.08	6.64
5.06	9	54.9	3.34	6.60
6.65	10	61.0	5.19	7.80
6.14	12	73.2	4.82	7.85
4.99	15	91.5	5.94	11.90
5.41	20	122	5.57	10.30
4.70	30	183	6.68	14.21

B. *Electron beam current = 20 mA*

Mass of target ($\times 10^{-7}$ kg)	Number of e-beam pulses	Total e-beam bombardment time (s)	Charge on target ($\times 10^{-12}$ C)	Charge-to-mass ratio ($\times 10^{-6}$ C/kg)
6.53	2	12.2	1.97	3.02
5.23	4	24.4	2.23	4.26
6.06	5	30.5	2.60	4.29
5.30	6	36.6	2.60	4.91
6.45	8	48.8	5.57	8.64
6.06	10	61	4.82	7.95
5.69	12	73.2	4.26	7.28
4.57	14	85.4	4.08	8.93
5.62	15	91.5	4.82	8.58
5.23	18	109.8	6.68	12.77
6.41	20	122	6.68	10.42
4.45	22	134.2	1.85	4.16

C. Electron beam current = 28 mA

Mass of target ($\times 10^{-7}$ kg)	Number of e-beam pulses	Total e-beam bombardment time (s)	Charge on target ($\times 10^{-12}$ C)	Charge-to-mass ratio ($\times 10^{-6}$ C/kg)
5.51	3	18.3	2.84	5.2
2.95	4	24.4	4.08	13.83
5.30	5	30.5	1.56	2.94
5.35	6	36.6	.59	.99
6.94	7	42.7	.93	1.34
6.22	8	48.8	2.60	4.18
5.99	9	54.9	5.57	9.30
4.89	10	61	1.86	3.80
4.83	11	67.1	2.34	4.84
5.55	12	73.2	5.57	10.04

2. *Charge on target vs. electron beam energy*

Electron beam current = 6 mA
Electron beam pulse duration = 6.1 s
Number of electron beam pulses = 30

Mass of target ($\times 10^{-7}$ kg)	Anode voltage (kV)	Charge ($\times 10^{-12}$ C)	Charge-to-mass ratio ($\times 10^{-6}$ C/kg)
6.03	1	2.41	4.00
6.26	2	4.64	7.41
5.06	3	5.45	10.77
4.70	3.9	6.68	14.21
4.99	5	7.42	14.87
5.03	6	7.79	15.49

3. Charge on target vs. pressure

Anode voltage = 3.9 kV
Electron beam pulse duration = 6.1 s
Number of charging pulses = 30
Electron beam current = 6 mA

Mass of target ($\times 10^{-7}$ kg)	Final pressure (torr)	Charge trapped in target ($\times 10^{-12}$ C)	Charge-to-mass ratio ($\times 10^{-6}$ C/kg)
4.70	1.0×10^{-5}	6.68	14.21
6.30	.01	8.05	12.78
5.51	.03	5.94	10.78
4.42	.1	4.08	9.23
5.48	.2	3.71	6.77
5.58	.5	1.86	3.33
5.84	.7	1.86	3.18
5.88	1.0	.37	.63

REFERENCES

1. T. B. Jones, G. A. Kallio, and K. S. Robinson, Polarized Particle Levitation in Hexapole Field, Colorado State University, Research Report No. 2 (1976).

2. S. Masuda, M. Washizu, and T. Sekiguchi, "Electrostatic Method of Pellet Handling," Proceedings, IEEE-IAS annual meeting, page 1005, Cincinnati, OH, Sept. 1980.

3. G. M. Sessler, In Electrets, ed. by G. M. Sessler (Springer-Verlag Berlin, 1980).

4. C. D. Hendricks, In Electrostatics and Its Applications, ed. by A. D. Moore (Wiley, New York 1973).

5. L. B. Loeb, Static Electrification (Springer, Berlin, 1958).

6. A. Y. Cho, J. Appl. Phys. 35, 2561 (1964).

7. S. Masuda and M. Washizu, J. of Electrostatics 6, 57 (1979).

8. M. M. Pauthenier and M. Moreau-Hanot, J. Physique Radium 3, 590 (1932).

9. G. M. Sessler and J. E. West, In Electrets, ed. by M. M. Perlman (Electrochemical Society, New Jersey, 1973).

10. M. J. Helix, Fabrication and Testing of Thin Silicon Windows for Electron Beam Transmission, M. S. Thesis, University of Illinois, 1976.

11. G. M. Sessler and J. E. West, J. of Electrostatics 1, 111 (1975).

12. B. Gross, G. M. Sessler, and J. E. West, J. Appl. Phys. 24, 351 (1974).

13. H. Frohlich, Proc. Roy. Soc. A188, 521 (1947).

14. A. Watson and J. Dow, J. Appl. Phys. 39, 5935 (1968).

15. B. Gross, J. Appl. Phys. 38, 2272 (1967).

16. J. E. Holliday and E. J. Sternglass, J. Appl. Phys. 30, 1428 (1959).

17. J. D. Cross and R. Blake, In Electrets, ed. by M. M. Perlman (Electrochemical Society, New Jersey, 1973).

18. K. R. Spangenberg, Fundamentals of Electron Devices (McGraw-Hill, New York, 1957).

19. J. J. O'Dwyer, The Theory of Dielectric Breakdown of Solids (Oxford University Press, Oxford, 1964).

20. J. R. Bayless, Plasma Cathode For E-Beams Lasers, Hughes Research Laboratories, Report AD-764 079 (1973).

21. D. J. Sturges and H. J. Oskam, J. Appl. Phys. 35, 2887 (1964).

22. G. M. Janney, J. R. Bayless and W. Clark, Plasma Cathode For E-Beam Lasers, Hughes Research Laboratories, Report N 00014-72-C-0496 (1975).

23. P. H. Ong and J. Van Turnhout, In Elektrostatische Anpladung (Verlag Chemic, Weinheim, 1974).

24. M. M. Perlman and S. Unger, Appl. Phys. Lett. 24, 579 (1974).

25. J. Van Turnhout, J. of Electrostatics 1, 147 (1975).

26. J. Van Turnhout, Thermally Stimulated Discharge of Polymer Electrets (Elserier, Amsterdam, 1979).